Trans Indian Inst Met
https://doi.org/10.1007/s12666-022-02789-x

ORIGINAL ARTICLE

Weld Strength and Microstructure Analysis on Resistance Spot Welding of Austenitic AISI 347 Stainless Steel and Duplex AISI 2205 Stainless Steel

M. Prabhakaran[1,2] · Jeyasimman Duraisamy[1] · N. Siva Shanmugam[3] · A. Rajesh Kannan[3] · M. Varatharajalu[4]

Received: 6 April 2022 / Accepted: 1 October 2022

Abstract In this research, the effect of welding current and heating cycle is studied against the weld strength. The AISI 347 and AISI 2205 of 2 mm thickness are taken for conducting the experiment. The squeezing time cycle, holding time cycle and electrode tip diameter are kept constant. The welded specimens are fractured using a tensile shear load testing facility and a macrograph examination is carried out. The specimen welded with the highest welding current of 8.5 kA and 14 heating cycles obtained the largest weld nugget and absorbed a maximum tensile shear load of 18.5 kN. All the samples except one failed under interfacial mode and sample 9 failed under pull-out failure mode. The scanning electron microscope (SEM) image of the failed nuggets shows a smooth transition from the austenitic to a mixture of austenitic–ferritic phase structures. The SEM–energy-dispersive spectroscopy analysis was carried out on the selected samples for their weld composition. The elemental spectrum shows a Cr_{eq}/Ni_{eq} ratio of 2.52 which confirms a ferritic phase formation upon solidification. The fractography results show the formation of dimples and torn bands on the lower and upper surfaces of the fractured nugget revealing the ductile failure of the weld. Maximizing the welding current and heating cycle maximizes the weld nugget area. The specimens which did not attain the minimum weld nugget size failed in the interfacial mode.

Keywords Resistance spot weld · AISI 347 · AISI 2205 · Duplex stainless steel · Tensile shear strength · Failure mode · EDS · Fractography

1 Introduction

Resistance spot welding (RSW) is a traditional and indispensable method of welding thin sheet metals and finds wide application in the aeronautical and automobile industries. Several methods are available for joining dissimilar metals, out of which the resistance spot welding is popularly used for several applications [1]. Austenitic stainless steel (ASS), which is non-magnetic and anti-corrosive, is highly ductile and easily weldable. It has better resistance to oxidation and intergranular corrosion. ASS is extensively used in chemical processing plants, petroleum refineries and waste heat recovery systems due to its high anti-corrosive property. Duplex stainless steel (DSS) consists of an equal amount of austenitic and ferritic phases in its composition. DSS exhibits very good chloride pitting and crevice corrosion resistance when compared with the 300 series of stainless steel. AISI 2205 goes well with AISI 347 in terms of welding properties.

Vigneshkumar M et al. [2] reviewed the challenges faced during the dissimilar spot welding of metals and revealed the benefits of dissimilar joints over similar joints with the limitation of the formation of brittle intermetallic phases. Biradar and Dabade [3] studied the role of the weld parameters on the dissimilar weld of mild steel (MS) and ASS 304. A mathematical model was developed to relate the weld parameters with the weld strength. In addition to the above

✉ Jeyasimman Duraisamy
jeyasimman76@gmail.com

1 Department of Mechanical Engineering, Periyar Maniammai Institute of Science & Technology, Vallam, Thanjavur 613 403, India

2 Department of Mechanical Engineering, Agnel Institute of Technology and Design, Assagao, Bardez, Goa 403 507, India

3 Department of Mechanical Engineering, National Institute of Technology, Trichy 620 015, India

4 Department of Mechanical Engineering, Sri Krishna College of Technology, Kovaipudur, Tamil Nadu 641 042, India

Published online: 28 October 2022

Table 1 Chemical composition of AISI 347 and DSS 2205

Name of the element	C	Mn	Si	Cr	P	Ni	S	Nb
AISI 347 composition (%)	0.08	2	0.75	19	0.045	0.02	0.03	1
DSS 2205 composition (%)	0.02	0.82	0.36	23	0.03	5.46	0.01	–

Table 2 – Mechanical Properties of AISI 347 and DSS 2205

Properties	Unit	AISI 347	DSS 2205
Yield strength (0.2%)	MPa	205	448
Tensile strength	MPa	525	621
Elongation	%	34	25
Hardness (HB)	HRB / HRC	87 HRB	31 HRC
Elasticity	GPa	201	190
Density	Kg/m^3	8000	7800

work, Watmon et al. [4] worked on RSW of 1 mm-thick mild steel sheet and investigated the variation in the mechanical properties due to the annular recesses on the copper electrode. Resistance spot welding of dissimilar stainless steel grades was carried out between SS304 and SS430 grades under various possible combinations [5]. The results of the study proved that the dissimilar welds exhibit higher hardness and toughness in comparison with similar metal welds. Similarly, research studies on dissimilar spot welding on various grades of duplex and martensitic stainless steel provide considerable information on dissimilar welding characteristics [6–9]. The investigations on RSW of quenched and partitioned (Q&P) steels and galvanized dual phase (DP) steels reported the hardness and strength of the welds at different critical heat-affected zones. But the RSW of Q&P steel with low-carbon steel suffers from liquid metal embrittlement on either side of the base metal [10, 11]. The addition of silicon to the DP steel up to 1.51 wt% considerably increases the peak load of failure but any further increase in silicon causes the peak failure load and fracture energy to drop drastically [12]. Investigative study on coated advanced high-strength steels (AHSS) was done by DiGiovanni et al. [13] in which experiments were conducted with and without zinc coating on the AHSS plates. The research concluded that the liquid metal embrittlement (LME) cracking is inevitable in the path towards fracture. It was observed that the surface modification of AHSS leads to a reduction in heat input due to oxide formation [14]. Das et al. [15] studied the dissimilar spot welding of AISI-1008 steel with Al-1100 alloy with graphene as interlayer and it revealed that the graphene coating causes a 124% enhanced strength. Resistance spot welding of dissimilar metals and their corresponding research have also been carried out. Shi et al. [16] made a detailed study on dissimilar RSW of aluminium to steel by varying the polarity on the aluminium sheet. The effect of the interlayer thickness on the mechanical properties of the RSW of aluminium with magnesium was studied and the results proved that the interlayer coating enhances the weld strength [17]. RSW of Al–Mg aluminium alloy with aluminium clad steel sheet was done and the results showed that the formation of intermetallic layer does not play any detrimental role in the weld strength [18]. The microstructural and mechanical study on RSW of modern materials was done by Chen et al. [19] in which five different bonding types were analysed. A. Maurya et al. [20] experimentally studied the effect of the filler material during the gas tungsten arc welding of DSS2507 with nitronic steel. The study on the microstructure and properties of the modern laser welding austenitic stainless steel and P91, P22 steels used for power plant applications was also carried out [21, 22].

In addition to the study on mechanical properties of the welded specimens, mathematical modelling of the weld parameters was done. Sheikhi et al. [23] researched the prediction model for nugget microstructure and hardness as a function of the weld cooling rate during the RSW of

Table 3 Experimentation based on DoE

Trial No.	Welding current (kA)	Squeezing time (cycles)	Heating time (cycles)	Holding time (cycles)	Electrode tip diameter (mm)
1	6.5	50	10	10	10
2	6.5	50	12	10	10
3	6.5	50	14	10	10
4	7.5	50	10	10	10
5	7.5	50	12	10	10
6	7.5	50	14	10	10
7	8.5	50	10	10	10
8	8.5	50	12	10	10
9	8.5	50	14	10	10

automotive steel sheets and Farrahi G et al. [24] compared the simulation and experimental results of RSW of three thin low-carbon steel sheets on the weld quality and the depth of electrode indentation on the nugget. Kumar et al. [25] did a numerical simulation 3D modelling of RSW of mild steel and stainless steel specimens and the model was found to have a strong correlation with experimental results. Aghajani H and Pouranvari [26] worked on creating a pathway to develop strong weld spots while RSW martensitic stainless steels. Pouranvari et al. [27] also contributed to the development of an approximation prediction model to analyse the modes of failure in the resistance spot welds of AHSS.

Stainless steel material in general and austenitic stainless steel in particular are preferred to serve corrosive and high-temperature service areas wherein the materials have to withstand a certain range of temperature for a prolonged period. The austenitic stainless steel is prone to undergo the phenomenon of sensitization in which the chromium carbide precipitates along the grain boundaries, when the material is subjected to a temperature range of 500–900 °C [28]. The niobium-stabilized AISI 347 stainless steel which prevents the chromium carbide precipitation is widely used for such service conditions than AISI 316. It is transparent from the past literature that, the experimentation and analysis of the weld characteristics of the dissimilar resistance spot welding of austenitic stainless steel AISI 347 with the duplex stainless steel AISI 2205 are in the infant stage. Therefore, the objective of this paper is to investigate the mechanical and microstructure properties of the dissimilar weld between the above-mentioned two different grades of stainless steel.

Fig. 1 Resistance spot welding machine

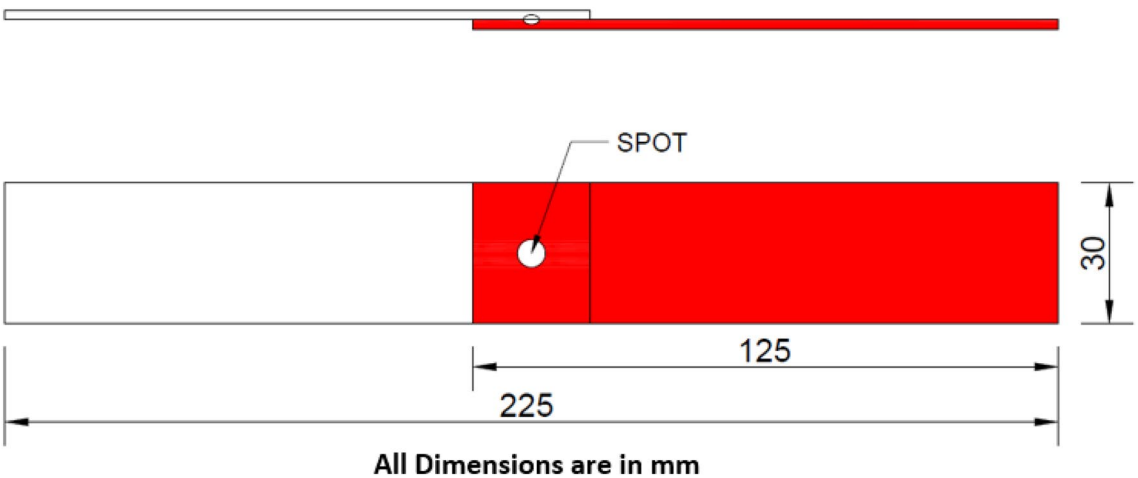

Fig. 2 Tensile shear test sample arrangement

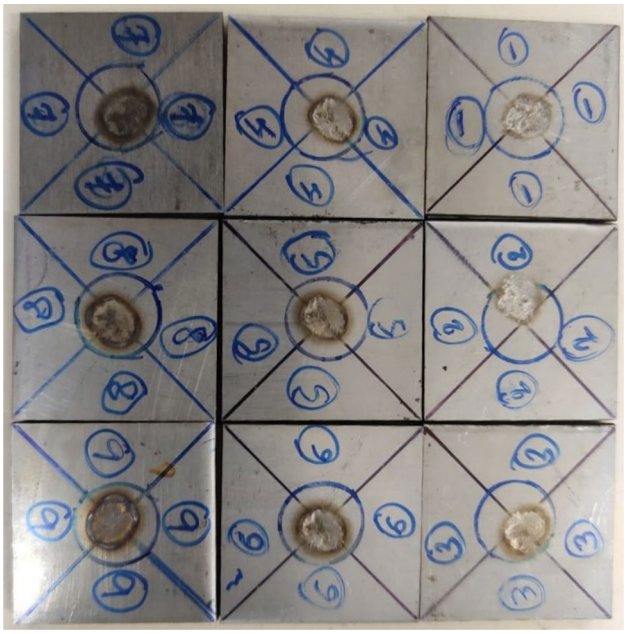

Fig. 3 Welded specimens

2 Materials and Methods

This work studies the dissimilar resistance spot welding of AISI 347 with AISI 2205. The dissimilar welding of duplex stainless steel with other grades of steel plays a critical role in the pressure vessels, superheaters, piping, turbine casing of power plant units and subsea manifolds [29]. The most significant reason for adopting dissimilar welding is to reduce the cost of fabrication by eliminating the expensive high-strength alloys for critical components [30]. The dissimilar welding of two different grades of steel or two different metals is a challenging task due to several reasons. When different grades of materials are involved, maintaining a balance in the physical, chemical and metallurgical properties during the welding and post-welding process is a highly impossible scenario [31]. A lot of metallurgical issues and defects are likely to occur if a dissimilar welding process is not carefully executed. In spite of these challenges, dissimilar welding is inevitable due to its overwhelming advantages. These challenges though cannot be totally avoided, it is possible to mitigate these effects by proper control of the weld parameters and post-treatment of the welding [32]. In this regard, it is very essential to carry out research on the RSW of various dissimilar metals. Hence in this study, the microstructure and mechanical properties of the dissimilar welding of austenitic AISI 347 and DSS 2205 are investigated in detail. As this pair of dissimilar metals has not been investigated in the literature, the research output of this study would be very significant for future researchers. Tables 1 and 2 show the chemical composition and the mechanical properties, respectively, of both the base metals.

Based on the preliminary trials carried out, the range of the welding current and heating cycle was decided. Then, within the decided range, 9 experimental trials were done as per the design of experiments (DoE) shown in Table 3, by varying the welding current and heating time cycles at three different levels. The squeezing time cycle, holding time cycle and electrode tip diameter was kept constant throughout the experiment. The resistance spot welding trials were carried out using the NASH 815 V2 microprocessor-controlled manual pedal-operated resistance spot welding machine shown in Fig. 1. The dimensions of the welding samples are shown in Fig. 2. The welded specimens are

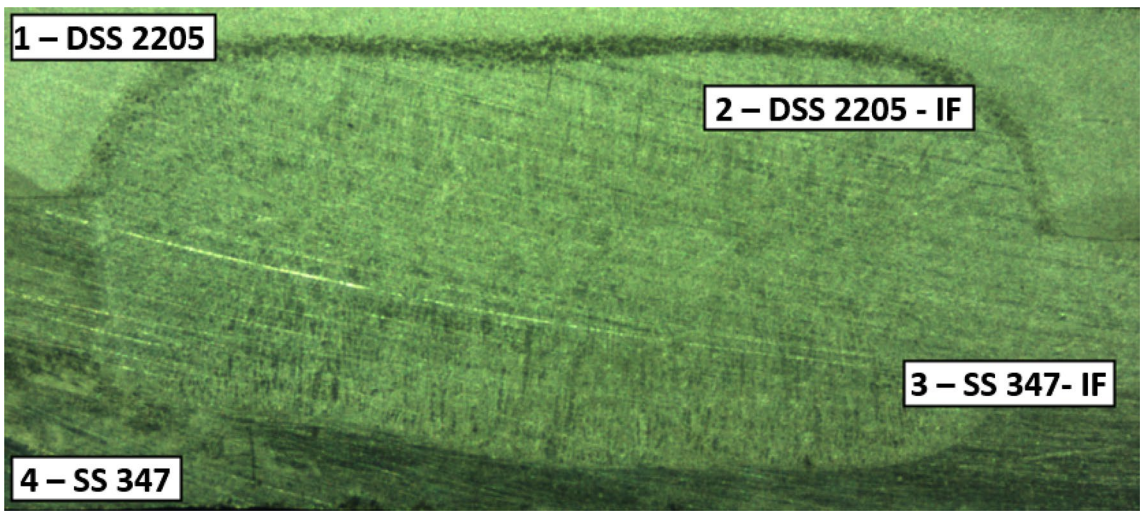

Fig. 4 Macrograph of welded specimen

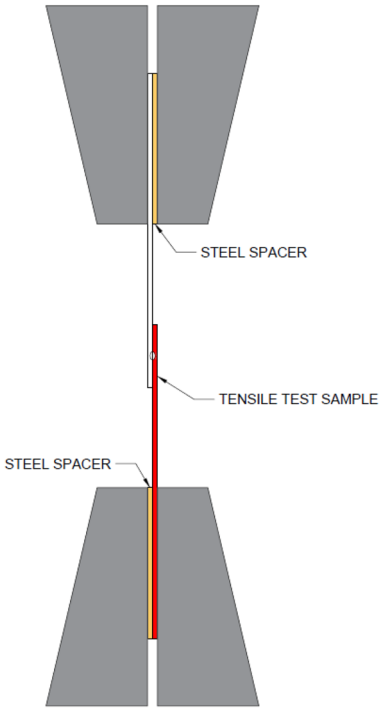

Fig. 5 Tensile shear testing mounting arrangement for weld specimen

shown in Fig. 3. After welding, the samples were cut across its cross section using wire cut electric discharge machining, to expose the weld nugget. The cut sections were macro-etched to expose the weld nugget for inspection. The macrograph examination shown in Fig. 3 reveals the quality of the weld nugget (Fig. 4). Further to assess the strength of the weld, the welded samples were fractured using Tinius Olsen H50KL Tensile Shear testing machine with a loading rate of 1 mm/min. The mounting arrangement of the tensile shear testing machine is shown in Fig. 5.

3 Results and Discussion

3.1 Macrograph Results

The welded specimens were subjected to macrograph analysis by sectioning the specimen along the centre of the weld, then polished with standard metallographic techniques and analysed with Welding Expert software. The weld macrograph examination results are reported in Table 4.

According to the American National Standard, the eligible nugget diameter for a given thickness '*t*' of a material is represented by the relation $4\sqrt{t}$ [6]. While studying the nugget diameter of the welded specimens, specimen 6, 8 and 9 has acquired a nugget diameter well above the threshold value of $4\sqrt{t}$. Hence out of the 9 specimens welded in

Table 4 Macrograph of weld nugget for various welding current and heating cycles

Welding current		6.5 kA	7.5 kA	8.5 kA
Heating cycles				
10 cycles	AISI 347	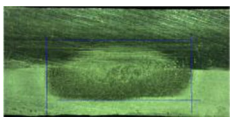	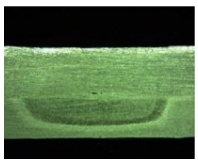	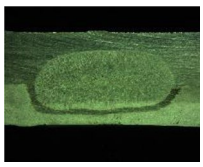
	DSS2205	Length = 4.8119 mm Thickness = 2.0094 mm	Length = 5.2308 mm Thickness = 1.8390 mm	Length = 5.2816 mm Thickness = 2.3158 mm
12 cycles	AISI 347	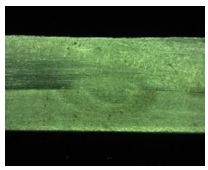	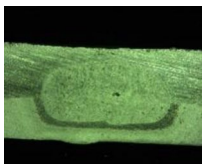	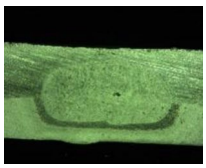
	DSS2205	Length = 2.0697 mm Thickness = 1.1088 mm	Length = 4.8607 mm Thickness = 2.3047 mm	Length = 5.9423 mm Thickness = 2.6864 mm
14 cycles	AISI 347	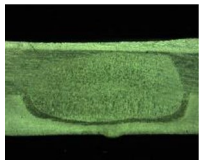	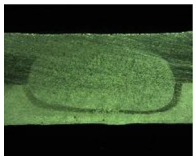	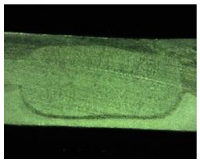
	DSS2205	Length = 3.8888 mm Thickness = 1.0938 mm	Length = 5.8221 mm Thickness = 2.3624 mm	Length = 6.1273 mm Thickness = 2.8049 mm

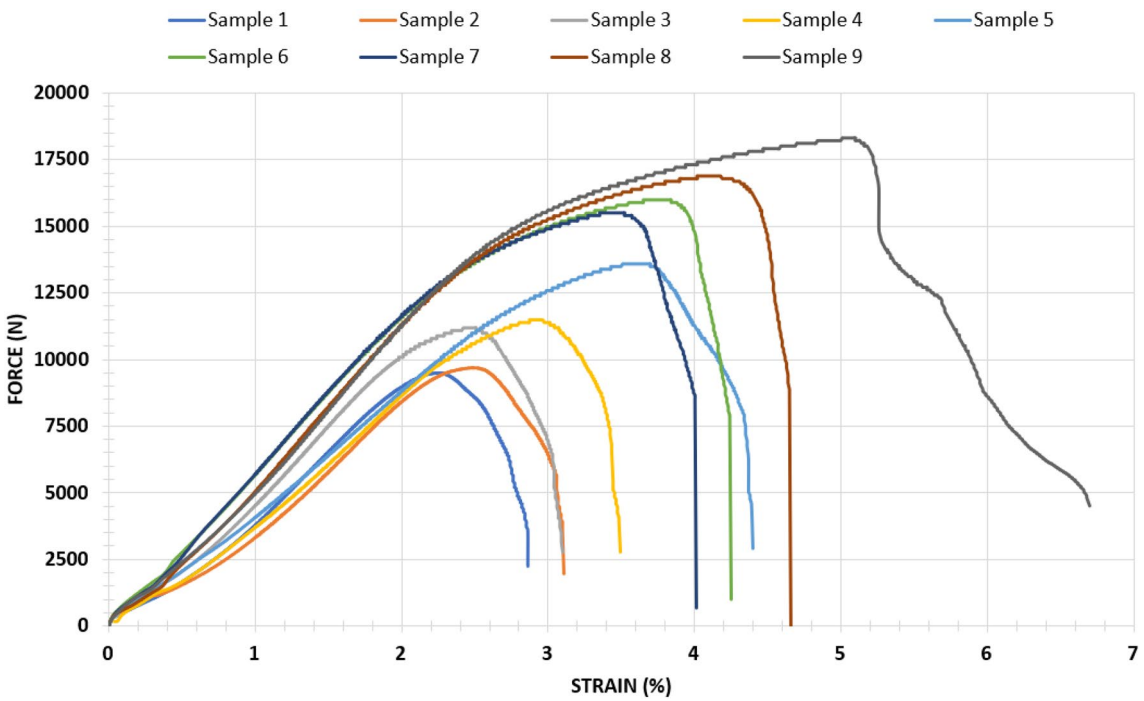

Fig. 6 - Tensile shear load–displacement curve

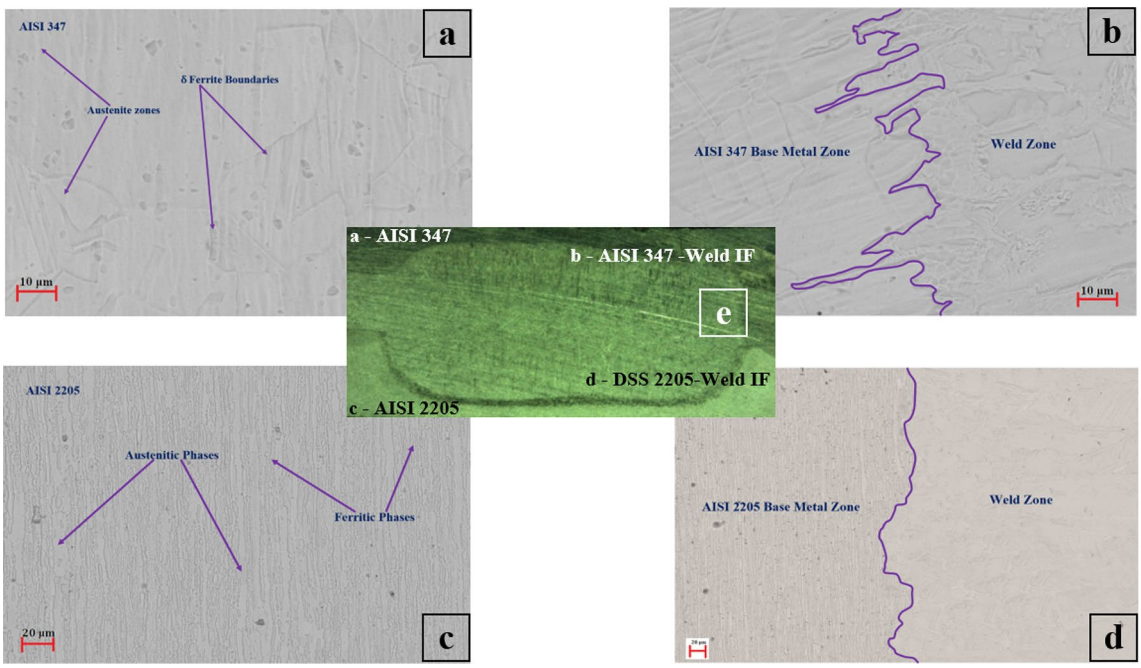

Fig. 7 **a** AISI 347 Base Metal Microstructure; **b** AISI 347—Weld Interface Microstructure; **c** AISI 2205 Base Metal Microstructure; and **d** AISI 2205—Weld Interface Microstructure

total, these 3 specimens qualify to be the eligible welds surpassing the minimum nugget diameter. To substantiate, the macrograph images in Table 4 and the tensile shear load–displacement curve in Fig. 6 can be correlated. The macrograph images of specimen 6, 8 and 9 shows that the nugget area is in an increasing pattern and their tensile shear load before failure is also in ascending order and sample 9

Fig. 8 Tensile shear test sample

Table 5 Ultimate tensile strength and joint efficiency

Trial no.	Ultimate tensile strength (MPa)	Joint efficiency w.r.t AISI 347 (%)	Joint efficiency w.r.t DSS 2205 (%)
1	158	30.10	25.44
2	161	30.67	25.93
3	186	35.43	29.95
4	191	36.38	30.76
5	227	43.24	36.55
6	267	50.86	43.00
7	258	49.14	41.55
8	281	53.52	45.25
9	304	57.90	48.95

has recorded a maximum failure load of 18.5 kN. When the welding current is kept to a maximum of 8.5 kA, an increasing trend can be witnessed in the nugget diameter with the increase in the heating cycles. In addition, upon observation of the weld lobes of the specimen welded with 6.5 kA welding current a poor depth of penetration is seen and has failed below 11 kN of tensile shear load. The nugget diameter increases with the increase in the heating cycle and the welding current and this conforms to the results obtained

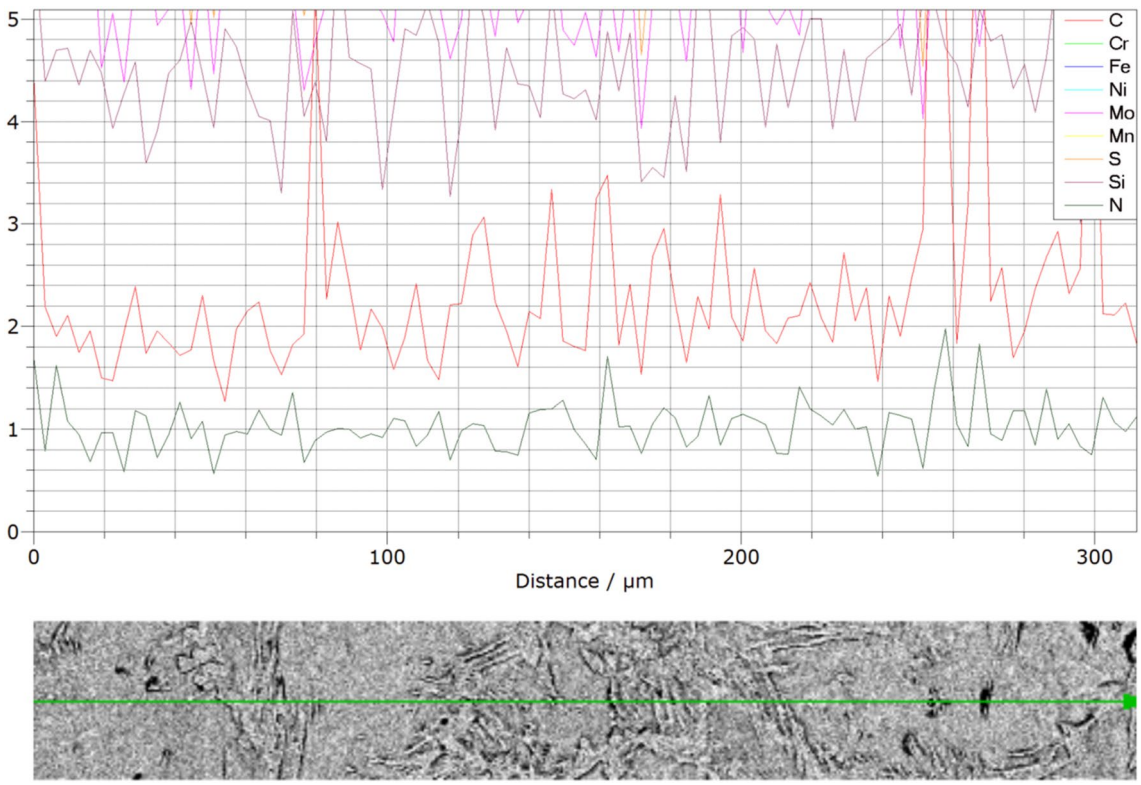

Fig. 9 EDS line scan of weld nugget

by Jagadeesha T during the experimentation of RSW of austenitic stainless steel [6, 9]. The weld nugget formed under 6.5 kA welding current has no clear demarcation of the weld lobe from the base metals.

3.2 Microstructure Analysis

Whenever it comes to the dissimilar RSW of two base metals, the formation of heat-affected zones (HAZ) adjacent to either side of the fusion zone is inherent. Hence dissimilar spot welding is always characterized by a fusion zone or weld zone, HAZ and base metal zone. The microstructure image shown in Fig. 7a shows the base metal on an austenitic background structure with grain boundaries of ferrite. The austenitic stainless steel in as welded condition has the tendency to produce delta ferrite boundaries [33]. The HAZ of the austenitic base metal as shown in Fig. 7b shows the presence of ferritic boundaries in the weld lobe [34]. The presence of ferritic structure can be seen to gradually increase from the base metal side to the interface region. This increase in the ferritic structure at the weld nugget region is accounted by the effect of an increase in the temperature and diffusion of AISI 2205 in the weld lobe. The microstructure of the second base metal AISI 2205 is given in Fig. 7c. Establishing austenitic–ferritic phase balance is one of the prominent issues while dealing with DSS [35]. The dendritic grain structure is the ferritic phase which is formed on the background of the austenitic phase. The microstructure of the interface region of the DSS with the weld lobe can be seen in Fig. 7d. The clear transition in the grain structure from the base metal region to the weld nugget region is due to the application of the electrode force and the heat cycles.

Vignesh K et al. [34] have also reported a similar behaviour of formation of delta ferrite in the austenitic steel region during the RSW SS 316L with DSS 2205. The austenitic phases reduce as the surface moves from the SS347 base metal region to the weld nugget and the combination of the ferritic dendrites with coarse austenite can be seen at the interface. This phenomenon is due to the diffusion of both

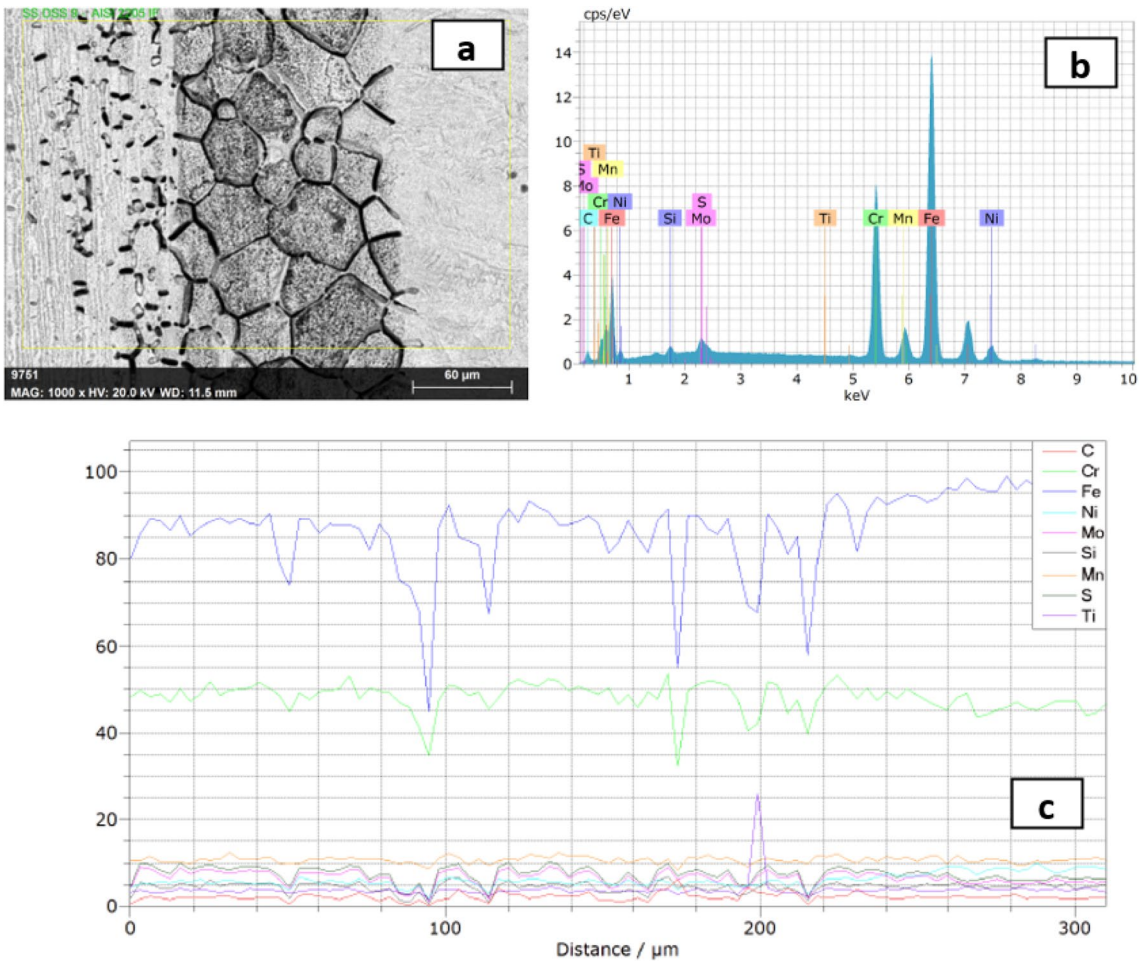

Fig. 10 DSS 2205 Interface with base metal: **a** Micrograph; **b** EDS spectrum; and **c** Line scan

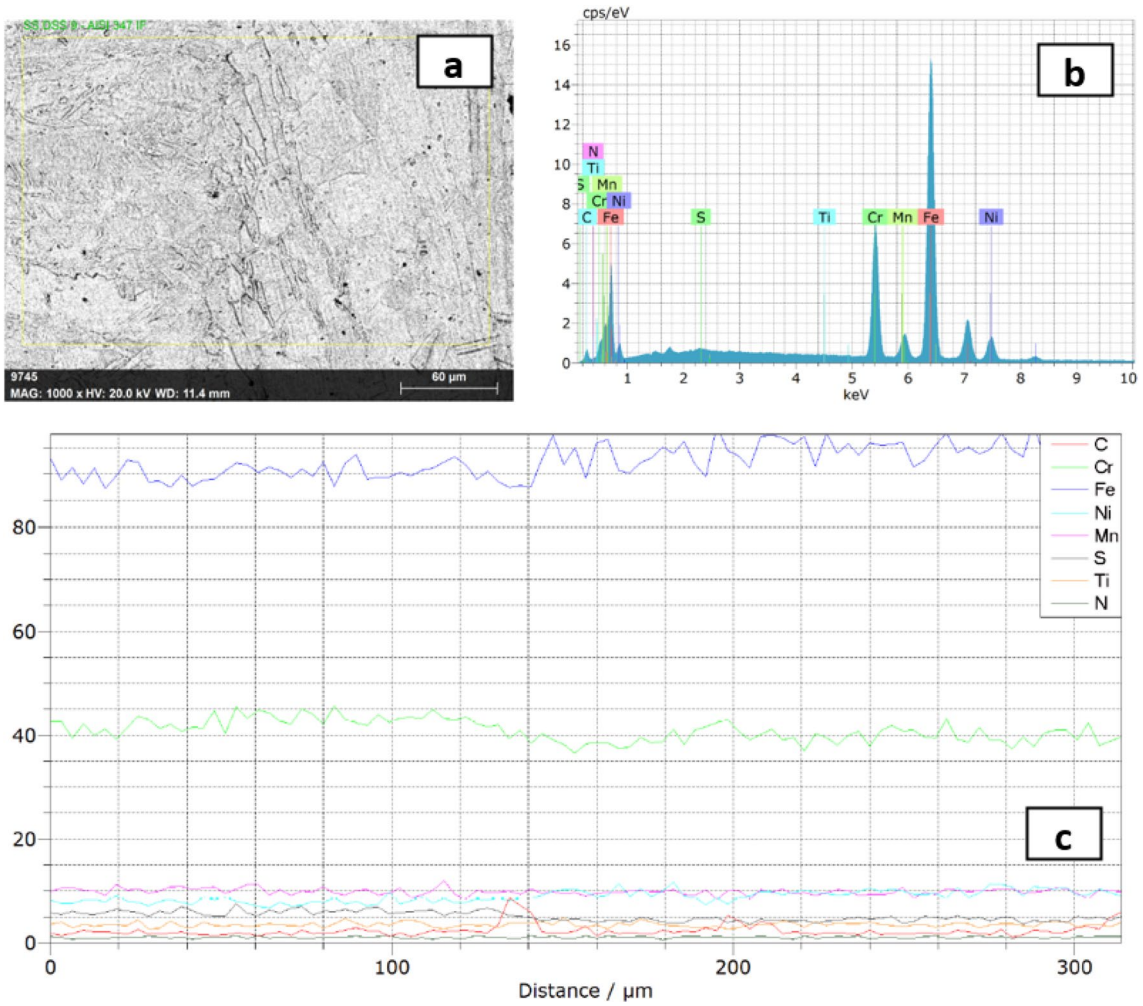

Fig. 11 AISI 347 Interface with base metal: **a** Micrograph; **b** EDS spectrum; and **c** Line scan

the parent metals at very high temperatures produced due to the heat cycles [36].

3.3 Tensile Shear Test and Failure Mode Analysis

The specimens for the tensile shear test were prepared as per the AWS standard 11.2.3.2.1. Fig. 6 shows the shear load–displacement curve of the various samples. The fractured samples of the tensile shear test are shown in Fig. 8. The shear stresses predominant at the weld nugget cause interfacial failure [6]. In this current research, the samples welded under 6.5 and 7.5 kA welding current have failed under interfacial mode and the sample welded under 8.5 kA have failed under pull-out mode [37]. The weld nuggets having a diameter less than the critical nugget diameter of $4\sqrt{t}$ which is 5.65 mm for the current study fail in interfacial mode. The weld nuggets that exceed this critical value, i.e. sample 9 having a nugget diameter of 6.127 mm, fail in pull-out mode after absorbing a maximum shear load of 18.3 kN and displacing 8.35 mm [38, 39]. The welding current and heating cycle for this sample are 8.5 kA and 14 cycles, respectively, which implies that as the welding current and the heating cycles are increased simultaneously, the weld nugget increases in size. This causes the weld nugget to absorb maximum shear load before failure [40]. Upon visually investigating the failure mode of the other samples welded below 8.5 kA have failed under interfacial mode [41]. The shear load data shows that the failure load keeps on increasing with the increase in welding current and heating cycles as the welding force and electrode tip diameter are kept constant. The increase in shear load can be attributed to welding current and heating cycles. Table 5 shows the ultimate tensile strength and the joint efficiencies of all the samples. Since the current research is focused on the dissimilar welding,

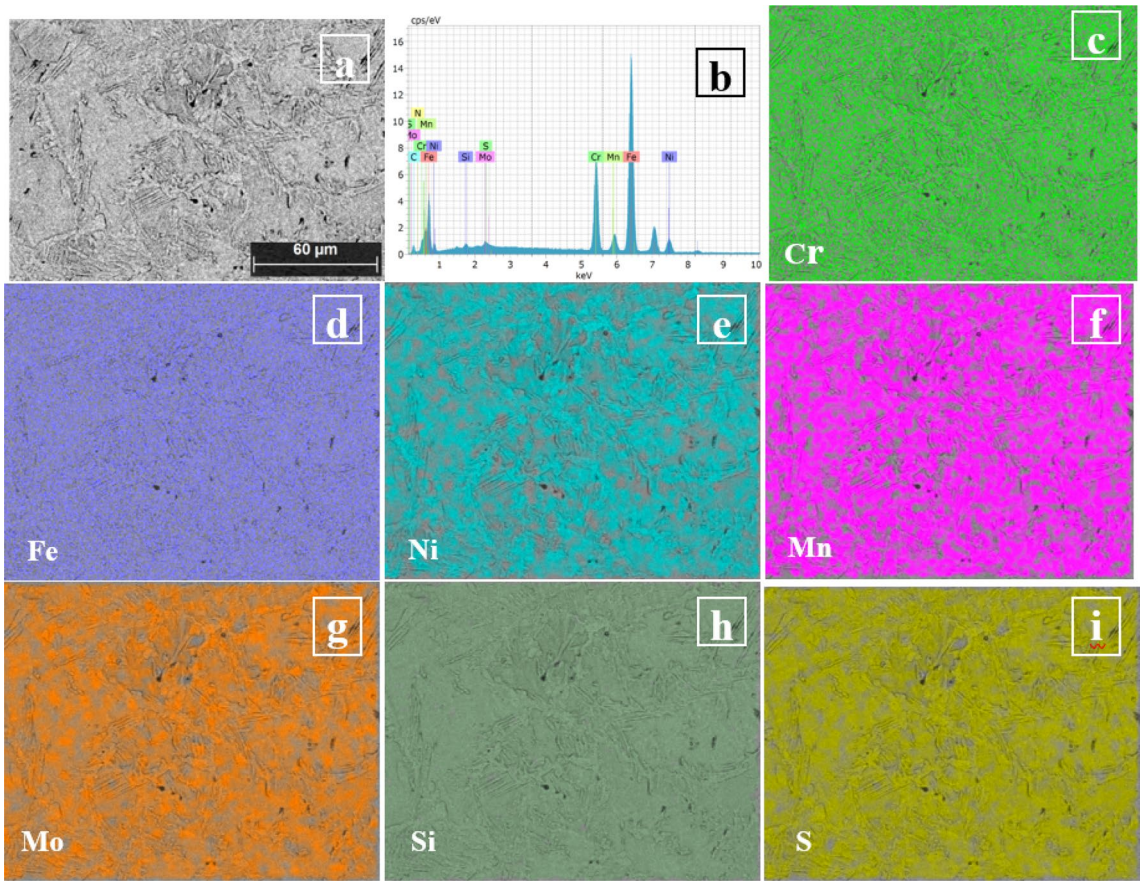

Fig. 12 EDS Elemental Mapping: **a** Weld zone Microstructure; **b** EDS Spectrum; **c** Chromium; **d** Ferrous; **e** Nickel; **f** Manganese; **g** Molybdenum; **h** Silicon; and **i** Sulphur

the joint efficiency is calculated by considering the ultimate tensile strength of both the base metals.

3.4 EDS Analysis

To study the metallurgical changes in the weld specimen after welding, an EDS study is made at four locations which are illustrated in Fig. 7. Location 'a' shows the base metal AISI 347, location 'b' shows the interface of the AISI 347 and the weld nugget shows the mixed structure of austenite and ferrite. Similarly, location 'c' shows the AISI 2205 base metal region, and location 'd' shows the interface of the AISI 2205 with weld nugget, where the ferritic structure tends to decrease and the austenitic patches begin to emerge. [42].

The EDS line scan shown in Fig. 9 renders information about the key metallic composition of the weld nugget. In Fig. 9, the EDS results of the midline of the weld zone have been presented. The weld interface, EDS spectrum and line scan, respectively, of the DSS 2205 base metal are shown in Fig. 10a, b and c. Similarly, the weld interface, EDS spectrum and line scan, respectively, of the AISI 347 base metal are shown in Fig. 11a, b and c.

Fig. 12a shows the microstructure of the midline of the weld nugget and Fig. 12b shows the elemental spectrum of the weld centre. In this current study, the Cr_{eq}/Ni_{eq} ratio is 2.52 which makes it very clear that the weld pool has solidified as ferrite and this inference is backed up by the spectrum results which show the highest weight percentage of 67.01 of ferrous in the weld composition [8]. Fig. 12c–i represents the elemental mapping of the weld nugget.

3.5 Fractography Analysis

The majority of the failure of the welded samples are due to interfacial mode except for one sample which has failed in the button pull-out failure mode. The interfacial failure of the weld is due to the poor shear strength of the weld nugget area at the interface region [7]. Sample 9 which failed under pull-out failure mode was subjected to fractography

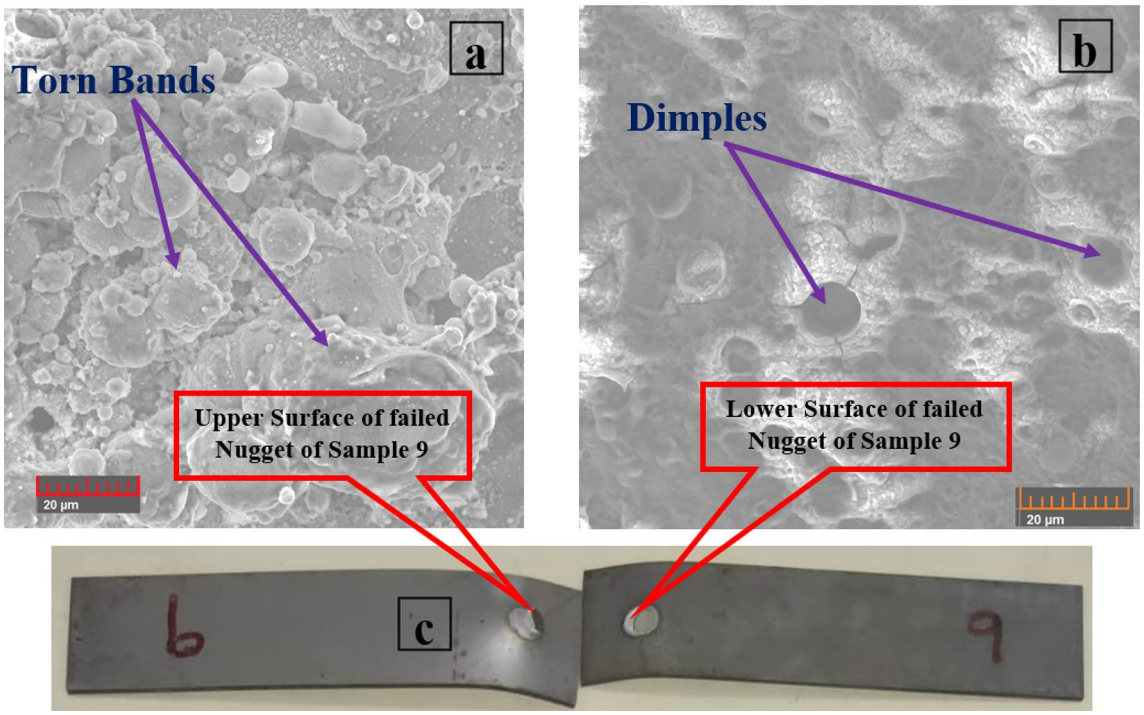

Fig. 13 SEM Fractography

analysis to understand its failure mechanism. Fig. 13 shows the fractography images of the failed sample 9. As seen in Fig. 13c, the weld nugget has undergone substantial plastic deformation due to the tensile load. The amount of plastic deformation that has occurred can be attributed to the soft nature of both the base metals. But the shearing of the sample has occurred around the circumference of the nugget, i.e. initiated from the HAZ of the base metal AISI 347 as austenitic stainless steels are less hard than the duplex ones[7]. The formation of the dimples and torn bands shown in Fig. 13a and b affirms the ductile nature of failure of the sample.

4 Conclusion

The following conclusions have arrived as an outcome of the research:

- The specimen welded with a welding current of 8.5 kA and 14 heating cycles possesses a maximum nugget diameter of 6.127 mm.
- The weld nugget area increases with an increase in the welding current and heating cycles.
- The application of the electrode force, heating cycles and the faster cooling rate of the spot welding process results in the transition of the microstructure of the base metals.
- The specimen welded with a maximum welding current and heating cycle exhibits a maximum displacement of 8.35 mm and fails at a maximum shear load of 18.3 kN.
- The weld specimen which attains a nugget diameter greater than $4\sqrt{t}$ fails through pull-out mode wherein all other specimens fail in interfacial mode.
- The weld zone has a Cr_{eq}/Ni_{eq} ratio of 2.52 and hence the solidification of the weld occurs in ferrite mode and this is confirmed by the EDS spectrum.
- The presence of the dimples and torn bands on the lower and upper surfaces of the failed weld nugget shows the ductile type of failure.

References

[1] Miyamoto K, Nakagawa S, Sugi C, Sakurai H, and Hirose A, Mater Des **165** (2019) 10785.https://doi.org/10.1016/j.matdes.2019.107585
[2] Vigneshkumar M, Mahandiran SB, Barath D, Dhyaneswar U, and Varun P (2021) Mater Today Proc https://doi.org/10.1016/j.matpr.2021.01.238
[3] Biradar AK, and Dabade BM, Mater Today Proc **26** (2019) 1284.
[4] Watmon TB, Wandera C, and Apora J, J Adv Join Process **2** (2020) 100035.https://doi.org/10.1016/j.jajp.2020.100035
[5 Zhang Y, Guo J, Li Y, Luo Z, and Zhang X, J Mater Res Technol 9 (2020) 574.https://doi.org/10.1016/j.jmrt.2019.10.086

[6] Krishnan V, Ayyasamy E, and Paramasivam V, Proc Inst Mech Eng Part E J Process Mech Eng **235** (2021) 12.https://doi.org/10.1177/0954408920933528
[7] Vignesh K, Perumal AE, and Velmurugan P, Arch Civil Mech Eng **19** (2019) 1029. https://doi.org/10.1016/j.acme.2019.05.002
[8] Arabi SH, Pouranvari M, and Movahedi M, Weld J **96** (2017) 307s.
[9] Jagadeesha T, Int J Adv Manuf Technol **93** (2017) 505. https://doi.org/10.1007/s00170-017-0517-5
[10] Ling Z, Wang M, Kong L, and Chen K, Mater Des **195** (2020) 109055. https://doi.org/10.1016/j.matdes.2020.109055
[11] Figueredo B, Chandran D, Andrew R, and Elliot M, Weld World **65** (2021) 2359. https://doi.org/10.1007/s40194-021-01179-z
[12] Badkoobeh F, Nouri A, Hassannejad H, and Mostaan H, Mater Sci Eng A **790** (2020) 139703. https://doi.org/10.1016/j.msea.2020.139703
[13] DiGiovanni C, Biro E, and Zhou NY, Sci Technol Weld Join **24** (2019) 218. https://doi.org/10.1080/13621718.2018.1518363
[14] Ghatei-Kalashami A, Zhang S, Shojaee M, Midawi ARH, Goodwin F, and Zhou NY, J Mater Process Technol **299** (2021) 117370. https://doi.org/10.1016/j.jmatprotec.2021.117370
[15] Das T, Das R, and Paul J J Manuf Process **53** (2020) 260. https://doi.org/10.1016/j.jmapro.2020.02.032
[16] Shi L, Kang J, Gesing M, Chen X, Haselhuhn AS, and Carlson BE, Int J Fatigue **141** (2020) 105866.https://doi.org/10.1016/j.ijfatigue.2020.105866
[17] Atieh AM, and Cooke K, Proc CIRP **96** (2021) 69.https://doi.org/10.1016/j.procir.2021.01.054
[18] Rahimi S, and Movahedi M, J Manuf Process **58** (2020) 429. https://doi.org/10.1016/j.jmapro.2020.08.026
[19] Chen G, Xue W, Jia Y, Shen S, and Liu G, Mater Sci Eng A **776** (2020) 776. https://doi.org/10.1016/j.msea.2020.139008
[20] Maurya AK, Pandey C, and Chhibber R, Arch Civ Mech Eng **22** (2022) 90. https://doi.org/10.1007/s43452-022-00413-9
[21] Sirohi S, Gupta A, Pandey C, Vidyarthy RS, Guguloth K, and Natu H, Optics Laser Technol **147** (2022) 107610. https://doi.org/10.1016/j.optlastec.2021.107610
[22] Dak G, Sirohi S, and Pandey C, Int J Press Vessels Pip **196** (2022) 104629. https://doi.org/10.1016/j.ijpvp.2022.104629
[23] Sheikhi M, Jaderian S, Mazaheri Y, and Pouranvari M, Sci Technol Weld Join **25** (2020) 511. https://doi.org/10.1080/13621718.2020.1747765
[24] Farrahi GH, Kashyzadeh KR, Minaei M, Sharifpour A, and Riazi S, Int J Eng Trans A Basics **33** (2020) 148.https://doi.org/10.5829/ije.2020.33.01a.17
[25] Kumar A, Panda S, Kumar Ghosh G, and Kumar Patel R, Mater Today Proc **27** (2019) 2958.
[26] Aghajani H, and Pouranvari M, Sci Technol Weld Join **24**(2019) 185. https://doi.org/10.1080/13621718.2018.1483065
[27] Pouranvari M, Marashi SPH, and Safanama DS, Mater Sci Eng A **528** (2011) 8344. https://doi.org/10.1016/j.msea.2011.08.016
[28] Kolli S, Javaheri V, Ohligschläger T, Kömi J, and Porter D, Mater Today Commun **24** (2020) 101088. https://doi.org/10.1016/j.mtcomm.2020.101088
[29] Sirohi S, Sauraw A, Kumar A, Kumar S, Rajasekaran T, Kumar P, Vidyarthy RS, Kumar N, and Pandey C, J Mater Eng Perform (2022). https://doi.org/10.1007/s11665-022-06747-y
[30] Sirohi S, Taraphdar PK, Dak G, Pandey C, Sharma SK, and Goyal A, Int J Press Vessels Pip **194** (2021) 104557. https://doi.org/10.1016/j.ijpvp.2021.104557
[31] Maurya AK, Pandey C, and Chhibber R, Int J Press Vessels Pip **192** (2021) 104439. https://doi.org/10.1016/j.ijpvp.2021.104439
[32 Pandey C, Mahapatra MM, Kumar P, Kumar P, Saini N, Thakare JG, and Kumar S, Eng Fail Anal **96** (2019) 158. https://doi.org/10.1016/j.engfailanal.2018.09.036
[33] Pandey C, Metall Mater Trans A Phys Metall Mater Sci **51** (2020) 2126. https://doi.org/10.1007/s11661-020-05660-0
[34] Vignesh K, Elaya Perumal A, and Velmurugan P, Int J Adv Manuf Technol **93** (2017) 455. https://doi.org/10.1007/s00170-017-0089-4
[35] Pouranvari M, Alizadeh-Sh M, and Marashi SPH, Sci Technol Weld Join **20** (2015) 502. https://doi.org/10.1179/1362171815Y.0000000015
[36] Bhat SD, Vijeesh V, Acharya P, and Rao M, (2020) Mater Today Proc **35** (2020) 365. https://doi.org/10.1016/j.matpr.2020.02.350
[37] Ma Y, Takikawa A, Nakanishi J, Doira K, Shimizu T, Lu Y, and Ma N, Mater Des **201** (2021) 109505. https://doi.org/10.1016/j.matdes.2021.109505
[38] Marashi P, Pouranvari M, Sanaee SMH, Abedi A, Abootalebi SH, and Goodarzi M, Mater Sci Technol **24** (2008) 1506. https://doi.org/10.1179/174328408X262418
[39] Chao YJ, Sci Technol Weld Join **8** (2003) 133.
[40] Mishra D, Rajanikanth K, Shunmugasundaram M, Kumar AP, and Maneiah D, Mater Today Proc **46** (2021) 919.
[41] Sobhani S, and Pouranvari M, Weld J **98** (2019) 263S. https://doi.org/10.29391/2019.98.023
[42] Mohammed HG, Ginta TL, and Mustapha M, Mater Today Proc **46** (2020) 1644. https://doi.org/10.1016/j.matpr.2020.07.258